

Boundary Effects on the Angle of Repose in Rotating Cylinders

Christian M. Dury and Gerald H. Ristow

Fachbereich Physik, Philipps-Universität, Renthof 6, 35032 Marburg, Germany

Jamie L. Moss and Masami Nakagawa

Division of Engineering, Colorado School of Mines, Golden, CO 80401, USA

(received 29 August 1997; revised March 24, 2022)

The angle of repose for the flow of granular materials in a half-filled rotating drum is studied by means of experiments and computer simulations. Particles of different material properties are used to investigate the effects of the end caps on the angle of repose. By fitting the numerical results to an exponentially decaying function, we are able to calculate the characteristic range, ζ , of the influence of the wall. We found that ζ scales with the drum radius but does not depend on either the density or the gravitational constant. For increasing particle diameter, finite size effects are visible.

46.10+z, 05.60.+w, 02.70.Ns, 81.05.Rm

I. INTRODUCTION

The behavior of granular materials is of great technological interest [1] and its investigation has a history of more than two hundred years. When granular materials are put in a rotating drum, avalanches are observed along the surface of the granular bulk [2,3]. In industrial processes, such devices are mostly used for mixing different kinds of particles. However, it is also well known that particles of different sizes tend to segregate in the radial and axial directions [4–14].

Recently, the particle dynamics of granular materials in a rotating drum has been described by using quasi two-dimensional systems, tracking individual grains via cameras and computer programs [9]. Extensive numerical studies have also reproduced and predicted many of the experimental findings [15–21]. The segregation and mixing process depends on many parameters, such as size [5,21], shape [19], mass [16], frictional forces, angular velocity [21], filling level of the drum [22], etc. The angle of repose of the material also depends on the parameters and it was argued that either the dynamic or static angle difference of the materials in the drum influence the axial segregation process [4,6,10,11].

In this article, we investigate experimentally the dependence of the dynamic angle of repose on the rotation speed of a half-filled drum for particles of different material properties. It is found that the angle is up to 5 degrees higher at the end caps of the drum due to boundary friction. Using a three-dimensional discrete element code, we are able to quantify this boundary effect and discuss its dependence on gravity, particle size and density.

II. EXPERIMENTAL RESULTS

An acrylic cylinder of diameter 6.9 cm and length 49 cm was placed horizontally on two sets of roller supports and was rotated by a well-regulated electronic motor. The material used was mustard seeds which are relatively round of average diameter about 2.5 mm, and have a coefficient of restitution, estimated from a set of impact experiments, of about 0.75 [23]. A set of experiments were conducted to measure the angle of repose in different flow regimes. For a small rotation speed, Ω , intermittent flow led to a different angle before and after each avalanche occurred, called the starting (maximum) and stopping (minimum) angle, respectively. For a larger rotation speed these intermittent avalanches became a continuous flat surface and thus enabled to define one angle of repose defined as the *dynamic angle of repose* as shown in Fig. 1a. When Ω increases, the flat surface deforms with increasing rotation speeds and develops a so-called S-shape surface for higher rotation speeds, shown in Fig. 1c. The deformation mostly starts from the lower boundary inwards and can be well approximated by two straight lines with different slopes close to this transition, sketched in Fig. 1b. For all measurements in this regime, we took the slope of the line to the right which corresponds to the line with the higher slope.

The average maximum and minimum angles of repose for the intermittent avalanches were found to be about 36 and 32 degrees, respectively, see Fig. 2. There seems to be a rather sharp transition from intermittent to continuous avalanches, which happens around $\Omega = 4$ rpm. For Ω greater than 4 rpm where the avalanches are continuous, the mustard seed data indicate a linear dependence of the dynamic angle of repose on the rotation speed which differs from the quadratic dependence found by Rajchenbach [3].

We also investigated the dynamic angle of repose for different particle diameters and materials in the continuous regime in more detail using a 27 cm long acrylic cylinder of diameter $2R = 6.9$ cm. For a given rotation speed, Ω , the dynamic angle of repose was measured four times at one of the acrylic end caps and the average value with an error bar corresponding to a confidence interval of 2σ , where σ is the standard deviation of the data points, was then calculated. First we used mustard seeds of two different diameters, namely 1.7 mm (black) and 2.5 mm (yellow), with a density of 1.3 g/cm³. The

latter were the same that were used to produce Fig. 2. We varied the rotation speed, Ω , from 5 rpm to 40 rpm and took the higher angle in the S-shaped regime which exists for higher rotation rates, see Fig. 1b. Both data sets are shown in Fig. 3 for black (\bullet) and yellow (\circ) seeds. The figure also illustrates the transition to the S-shaped regime which occurs at the change of slope, e.g. at around 11 rpm for the smaller seeds and around 16 rpm for the larger seeds. One also notes that the dynamic angle of repose is much higher for the larger particles in the low frequency regime. For values of $\Omega > 15$ rpm in the S-shaped regime, the difference in the dynamic angle of repose for the two different types of mustard seeds decreases with increasing Ω , and both curves cross around 30 rpm giving a slightly higher angle for the smaller seeds with the highest rotation speeds studied.

We applied the same measurements to two sets of glass beads having a density of 2.6 g/cm^3 . The smaller beads had a diameter of 1.5 mm with no measurable size distribution, whereas the larger beads had a diameter range of $3.0 \pm 0.2 \text{ mm}$. Both data sets are shown in Fig. 4 for small (\bullet) and large (\circ) beads. It can be seen from this figure that the transition to the S-shaped regime occurs at around 16 rpm for the smaller beads and around 24 rpm for the larger beads. In general, we found that the small particles exhibit the S-shaped surface at lower values of Ω than the large particles. The angles of repose are, in general, lower for the glass beads compared to the mustard seeds which we attribute to the fact that the mustard seeds are not as round as the glass beads and rotations of the mustard seeds are therefore more suppressed. The coefficient of friction is also higher for mustard seeds.

There are two striking differences when comparing Figs. 4 (glass spheres) and 3 (mustard seeds). For rotation speeds, Ω , lower than 15 rpm, the small and large glass beads have the same dynamic angle of repose which agrees with the findings in [24], whereas the dynamic angle of repose is significantly higher (3 to 4 degrees) for the larger mustard seeds compared to the smaller ones. For rotation speeds, Ω , higher than 15 rpm, the smaller glass beads show a higher dynamic angle of repose than the larger glass beads, and this angle difference increases with increasing rotation speed. For mustard seeds, the difference in the dynamic angle of repose between the smaller and the larger particles decreases with increasing Ω and the smaller seeds only show a higher angle for the highest rotation speeds studied. Both Fig. 3 and Fig. 4 seem to indicate that the increase in the dynamic angle of repose with rotation speed, Ω , in the S-shaped regime is larger for the smaller particles.

All the above angle of repose were measured by looking through one of the acrylic end caps. In order to study the boundary effect of these end caps on the dynamic angle of repose, we performed Magnetic Resonance Imaging (MRI) measurements. This technique of studying non-invasively the flow properties of granular materials was first used by Nakagawa et al. [23] and is in addi-

tion explained in more detail in ref. [7]. We used the large mustard seeds, which had an average diameter of 2.5 mm. The dynamic angle of repose was measured based on the concentration data which was averaged in a thin cross-sectional slice in the middle of the cylinder far away from the end caps. It is shown in Fig. 5 as function of the rotation speed by the open circles (\circ). We restricted the measurement to the flat surface regime, and all data points then lie approximately on a straight line. On the other hand, non-MRI data were measured at the end caps and are shown as stars (\star) in Fig. 5. The consistently higher dynamic angle of repose at the end cap indicates the significance of the friction between particles and the boundary wall. We also found that the S-shape regime seems to start earlier at the end caps due to the additional wall friction.

III. SIMULATION TECHNIQUE

When measuring the dynamic angle of repose for different materials at the end caps, we found that the angle is always lower in the middle of the drum and the influence of the end caps seems to be rather short range, the angle drops to the value in the middle of the drum within a few centimeters. We are particularly interested in the dependence of this length scale on the particle diameter and density and on the gravitational force. Since we only have a limited number of particle diameters and density available in the experiment, we use three-dimensional discrete element methods, also known as *granular dynamics*, to overcome this problem.

Each particle i is approximated by a sphere with radius r_i . Only contact forces during collisions are considered and the particles are not allowed to rotate. Since the mustard seeds are slightly aspherical, they rotate much less than glass beads. This was the motivation for our non-rotating assumption. The forces acting on particle i during a collision with particle j are

$$F_{ij}^n = -\tilde{Y} (r_i + r_j - \vec{r}_{ij} \cdot \hat{n}) - \gamma_n \vec{v}_{ij} \cdot \hat{n} \quad (1)$$

in the normal direction (\hat{n}) and

$$F_{ij}^s = -\min(\gamma_s \vec{v}_{ij} \cdot \hat{s}(t), \mu |F_{ij}^n|) \quad (2)$$

in the tangential direction (\hat{s}) of shearing. In Eqs. (1) and (2), γ_n and γ_s represent a dynamic friction force in the normal and tangential direction, respectively, \vec{r}_{ij} represents the vector joining both centers of mass, \vec{v}_{ij} represents the relative motion of the two particles, and \tilde{Y} is related to the Young's Modulus of the investigated material. Dynamic friction in the model is defined to be proportional to the relative velocity of the particles in the tangential direction.

During particle-wall contacts, the wall is treated as a particle with infinite mass and radius. In the normal direction, Eq. (1) is applied, whereas in the tangential direction, the static friction force

$$\tilde{F}_{ij}^s = -\min(k_s \int \vec{v}_{ij} \cdot \hat{s}(t) dt, \mu |F_{ij}^n|) \quad (3)$$

is used. This was motivated by the observation that when particles flow along the free surface, they dissipate most of their energy in collisions and can come to rest in voids left by other particles. This is not possible at the flat drum boundary. In order to avoid additional artificial particles at the walls which would make the simulations of three-dimensional systems nearly infeasible, we rather use a static friction law to avoid slipping and allowing for a static surface angle when the rotation is stopped. Both tangential forces are limited by the Coulomb criterion which states that the magnitude of the tangential force cannot exceed the magnitude of the normal force multiplied by the friction coefficient μ . For particle-particle collisions we use $\mu = 0.2$, and for particle-wall collisions, $\mu_w = 0.4$. In order to save computer time, we set \tilde{Y} to $6 \cdot 10^4$ Pa m which is about one order of magnitude softer than vulcanite but the maximal overlap of two particles is at most 0.3% of the sum of their radii, which is still realistic. This gives a contact time during collisions of $1.1 \cdot 10^{-4}$ s. The coefficient of restitution for wall collisions is set to 0.77 which is within the error bar of the experimentally measured value of 0.75, see section II. In experiments with spherical liquid-filled particles, we found only a weak dependence of the restitution coefficient on particle size and therefore used a normal force law, Eq. (1), that would make the restitution coefficient independent of particle size. When the same type of force law is applied to particle-particle collisions, it gives a normal restitution coefficient of 0.56. A discussion of the different force laws is given in ref. [25] and a review of different applications using granular dynamics is given in [26]. Even though detailed experiments for binary collisions of particles were performed, the force relations before and after a collision depend on the material and the asphery of the particles [27] and since these two quantities were not available for mustard seeds, we can only take the published values as a guideline. The numerical parameters were fine adjusted by comparing the experimentally determined dynamic angle of repose for 2.5 mm mustard seeds ($\rho = 1.3$ g/cm³) with the simulation results over the Ω -range from 8 to 35 rpm. The radius of the drum was chosen as $R = 3.5$ cm. Both data sets are shown in Fig. 6. Also shown as a solid line in Fig. 6 is the theoretical result based on a model by Zik et al. [24]. They started from the equilibrium condition for the surface flow j in a laminar and thin layer inclined with an angle Θ :

$$j = \frac{\rho g}{3\eta} h_0^3 \cos \Theta (\tan \Theta - \tan \Theta_0) \quad (4)$$

where ρ denotes the particle density, g gravity, η the constant viscosity and $\Theta_0 = \arctan \mu$. The cut-off depth, h_0 , corresponds to a constant pressure value of $p_0 = h_0 g \cos \Theta$. A second expression for the surface flow in a half-filled drum can be obtained by looking at mass conservation, [3]:

$$j = \rho \frac{\Omega}{2} (R^2 - r^2) \quad (5)$$

where r measures distance from the drum center along the free surface. Equating expressions (4) and (5) and using the relation $\tan \Theta = \frac{dy}{dx} = y'$, where $y(x)$ measures the height of the top surface particle along the surface and $(\cos \Theta)^{-1} = \sqrt{1 + (y')^2}$, we obtain

$$(y')^3 - (y')^2 \tan \Theta_0 + y' + c\Omega(y^2 + x^2 - R^2) = \tan \Theta_0 \quad (6)$$

with $c = \frac{3\eta g^2}{2\rho p_0^3}$. Corrections to this model were recently proposed by Khakhar et al. [28], but they lead to the same equations for the dynamic angle of repose as above in the case of a half-filled drum due to the symmetry of the thickness of the fluidized layer for shear flow. Solving for y' at the origin (drum center), the only one of the three roots with no imaginary part reads

$$y' = \tilde{\mu} + (B + \sqrt{D})^{1/3} - \frac{1/3 - \tilde{\mu}}{(B + \sqrt{D})^{1/3}} \quad (7)$$

where $3\tilde{\mu} = \tan \Theta_0$,

$$B = \tilde{\mu}(1 + \tilde{\mu}^2) + \frac{1}{2}c\Omega R^2 \quad \text{and} \\ D = 3(\tilde{\mu}^2 + \frac{1}{9})^2 + \tilde{\mu}(1 + \tilde{\mu}^2)c\Omega R^2 + (\frac{1}{2}c\Omega R^2)^2.$$

We integrated Eq. (6) numerically and checked that the theoretical profile has a similar shape for different rotation speeds as the numerical data. We adjusted the parameter c using the experimental data points and the best fit was obtained for $c = 0.0111 \pm 0.0001$ s/m² and $\mu = 0.51 \Rightarrow \Theta_0 = 27^\circ$. It is remarkable how well the theoretical curve fits the data points from the experiments and the numerical simulations, as shown in Fig. 6. The theoretical curve is very close to the arcus-tangent curve proposed by Hager et al. [29] and also found in two-dimensional simulations over a wide Ω -regime [30]. For low rotation speeds, $\Omega < 8$ rpm, the experiment is very near the discrete avalanche regime, and therefore the simulations where we have used only dynamic friction for the particle-particle interactions and the theory where a steady flow is assumed tend to deviate slightly from the experiment. Rajchenbach experimentally found the relation $\Omega \sim |\Theta - \Theta_c|^m$ with $m = 0.5$ leading to $\Theta = \Theta_c + \alpha\Omega^2$ [3] which gives an increasing slope for increasing Ω in the graph, whereas the experimental data points in our Fig. 6 suggest a decreasing slope with increasing Ω . To illustrate this point further, we replotted all of our available experimental data points of the large mustard seeds measured at the end caps, taken from Fig. 3 above, in the same fashion as Rajchenbach and obtained a scaling exponent of $m=0.87$ using $\Theta_c = 34.1^\circ$. This has to be compared with $m=0.5$ found by Rajchenbach and $m=0.7$ given by the numerical prediction by

Tang and Bak [31]. The Ω range of Rajchenbach is smaller than the one investigated by us and we speculate that his finding is valid close to the transition point to the continuous flow regime where the quadratic fit works rather well. We included this in Fig. 6 as dotted line using a best quadratic fit for the value of $\Omega < 20$ rpm.

IV. BOUNDARY EFFECT ON SURFACE ANGLE

As shown in Fig. 5, the dynamic angle of repose of granular material in a rotating drum is significantly higher at the end caps than in the middle. For the experimentally investigated particle sizes of the order of millimeter, the effect was visible up to a few centimeters. But this length scale might depend on the particle diameter and density and also on external parameters like gravity.

Using the above described technique, we simulated extended three-dimensional, half-filled drums. For a particle size of 2.5 mm and a rotation speed of 20 rpm, the time-averaged angle, denoted by $\langle\Theta(z)\rangle$, as function of the position along the rotation axis is shown in Fig. 7. Each point with corresponding error bar stands for a weighted average over the nearest neighbours. In order to study the characteristic length, ζ , of the boundary effect, we fit all data points by the relation

$$\langle\Theta(z)\rangle = \Theta_\infty + \Delta\Theta \left(e^{-z/\zeta} + e^{-(L-z)/\zeta} \right) \quad (8)$$

where L stands for the length of the drum, Θ_∞ for the dynamic angle of repose far away from the boundaries and $\Delta\Theta$ for the angle difference between the value at the boundary and Θ_∞ . For the curve shown in Fig. 7, the corresponding values are $\Delta\Theta \approx 4^\circ$, which is the same value given in Fig. 5 for the MRI experiment, $\zeta = 3.19 \pm 0.25$, $L = 20.6$ cm and $\Theta_\infty = 35^\circ \pm 0.2^\circ$. We tested Eq. (8) against the simulation results for different drum lengths of $L/2$, $L/4$ and $L/8$ and found a remarkably good agreement. In the last two cases, the value for Θ_∞ is never reached in the middle of the drum due to the boundary effects.

Using drums that are at least 64 particle diameters long, we studied the dependence of Θ_∞ (middle) and the angle at the end caps on the particle diameter d at the same rotation speed of 20 rpm. The simulation values in the tangential direction were chosen in such a way that the normalized tangential velocities before and after impact were *independent* of the particle diameter d . The ratio \tilde{Y}/k_s was set to 3.1, a value which gives for acetate spheres a good agreement of simulations [25] and experiments [27]. The value of γ_s was chosen sufficiently high to give a similar behavior in particle-particle- and particle-wall-collisions in the sliding regime. The results for the surface angle along the rotation axis are shown in Fig. 8, which illustrates that the angle increases with increasing particle size in agreement with the mustard seed

experimental results given in Fig. 3. The angle difference of around 4 degrees, which seems to be independent of the particle size, also agrees with the experimental findings. In other experiments, different dependencies were observed: das Gupta et al. [6] mostly found a higher angle for smaller particles using sand grains and Hill and Kakalios [10] measured higher angles for smaller particles when using sand and glass particles although it was also possible to get no angle difference for certain size ratios of glass spheres. The latter was also found by Zik et al. [24], whereas Cantelaube [32] did not find a clear trend when using discs in a quasi two-dimensional drum. What causes the different behaviour is not clear at the moment and a more detailed analysis would be desirable but is beyond the scope of this article. It is necessary to use appropriate values for the simulation parameters to quantitatively model a desired system, which is why we gathered as much information for the mustard seeds as possible. A arcus-tangent fit which gave a smaller mean deviation than a parabolic fit was added to Fig. 8 to guide the eye. Changing the density, ρ , of the particles or the gravitational constant, g , has a dramatic effect on the angle of repose: for the latter quantity this is shown in table I and a similar behaviour was seen in recent experiments [33]. For both ρ and g , an increase in value corresponds to an angle decrease. When a hydrostatic pressure, $p_0 \sim g$, is assumed, the data for $g < 30$ m/s² can be well described by Eq. (7). The lower g becomes the more pronounced the S-shaped surface becomes, and in the limit $g \rightarrow 0$, the transition to the centrifugal regime takes place at

$$\Omega_c \approx \sqrt{\frac{\sqrt{2}g}{R \sin \Theta_0}}$$

where Θ_0 denotes the average angle in the limit $\Omega \rightarrow 0$ [15,30]. In our case, for $\Omega = 20$ rpm the transition to the centrifugal regime occurs at $g \approx 0.45$ m/s², which is in perfect agreement with the numerical findings. Even though we studied more than one (two) orders of magnitude in ρ (g), we could not obtain an accurate infinite value limit.

V. RANGE OF BOUNDARY EFFECT

In order to study the range of the boundary effect, we extracted figures similar to Fig. 7 from our simulations and varied the drum length, L , and radius, R , the particle diameter, d , and density, ρ , the gravitational constant, g , and the rotation speed, Ω . The data points for the dynamic angle of repose as a function of position along the rotation axis were fitted by Eq. (8) giving the characteristic length, ζ , of this run. As expected, ζ did not vary when the length of the drum or the rotation speed was changed, but surprisingly, the characteristic length, ζ , did not change when the density of the particles or the

gravitational constant was changed by more than one order of magnitude, even though the dynamic angle of repose strongly depends on both as shown in table I for the latter quantity.

Based on the definition of ζ in Eq. (8), one might speculate that $\zeta \sim R$ since the gradient of the slope along the rotational axis of the surface should be a material property, i.e. it should not depend on the geometry. The angle of repose is independent of the drum radius, R , and therefore the height difference between the surface at the end cap and the surface in the middle of the drum must be proportional to R . This leads to $\zeta \sim R$ which is indeed the case, and we show in Fig. 9 the dimensionless characteristic length, ζ/R , as function of dimensionless particle diameter, d/R , for three different drum radii. Below a critical diameter, d_c , ζ seems to be independent of the particle size, and we propose the following relation

$$\zeta = \begin{cases} \alpha R & , \text{ if } d \leq d_c \\ \alpha R + \beta(d - d_c) & , \text{ if } d > d_c \end{cases} \quad (9)$$

where, in our case, $\alpha = 0.28$ and $\beta = 3.13$. The critical particle diameter $d_c \approx 0.14 R$ and it seems to decrease slightly with increasing drum radius. Therefore, particles in the fluidized zone with $d < d_c$ might be describable by a continuum model. For particles with $d > d_c$, we have to take finite size effects into account.

For comparison, we replot in Fig. 10 the data from Fig. 9 by showing the characteristic length, ζ , made dimensionless by the average particle diameter, d . A strong decrease in ζ/d and a later saturation is clearly visible for increasing particle diameter. The solid line is an exponential fit which matches all data points very well but it can only serve as a guide to the eye since it does not reproduce the right value in the limit $d \rightarrow 0$.

VI. CONCLUSIONS

We have investigated the dynamic angle of repose, Θ , in a three-dimensional rotating drum in the continuous flow regime. By choosing different materials and particle diameters, we discussed the Ω -dependence of Θ for glass beads and mustard seeds of two different sizes. In the low rotation speed regime, both types of glass beads showed the same angle of repose, whereas the angle was higher for the *larger* mustard seeds. Using MRI techniques, we could quantify, for the large mustard seeds, the angle difference between the middle and the end of the drum and its Ω -dependence. In all cases, either a linear or an arcus-tangent dependence of Θ on Ω was found. In order to investigate the range, ζ , of the boundary effects, we used a three-dimensional *discrete element* code and fitted the averaged angle along the rotation axis to two exponentially decaying functions. We found that ζ scales linearly with the drum radius. On the other hand, it does not depend either on the particle density or the gravitational

constant, even though the surface angle changes drastically with these quantities, or on the rotation speed of the drum. A detailed analysis of the dependence of the characteristic length, ζ , on the particle diameter, d , revealed that ζ is independent of d for small particle diameters but shows finite size effects for larger d .

ACKNOWLEDGMENTS

CMD and GHR gratefully acknowledge financial support by the Deutsche Forschungsgemeinschaft and partial funding for their stay in Golden by the *Particulate Science & Technology Group* of the Colorado School of Mines. JLM and MN are supported in part by NASA through contract number NAG3-1970. We also would like to thank Susan McCaffery for a critical reading of the manuscript. A generous grant of computer time on the Cray T3E at the Forschungszentrum Jülich made the numerical simulations possible.

-
- [1] H. M. Jaeger, S. R. Nagel, and R. P. Behringer, *Physics Today* **4**, 32 (1996).
 - [2] P. Evesque and J. Rajchenbach, *C.R. Acad. Sci. Paris, Série II* **307**, 223 (1988).
 - [3] J. Rajchenbach, *Phys. Rev. Lett.* **65**, 2221 (1990).
 - [4] M. B. Donald and B. Roseman, *Br. Chemical Engineering* **7**, 749 (1962).
 - [5] J. Bridgewater, *Powder Technol.* **15**, 215 (1976).
 - [6] S. Das Gupta, D. V. Khakar, and S. K. Bathia, *Chem. Engineering Science* **46**, 1513 (1991).
 - [7] M. Nakagawa, *Chem. Engineering Science-Shorter Communications* **49**, 2544 (1994).
 - [8] E. Clément, J. Rajchenbach, and J. Duran, *Europhys. Lett.* **30**, 7 (1995).
 - [9] F. Cantelaube and D. Bideau, *Europhys. Lett.* **30**, 133 (1995).
 - [10] K. M. Hill and J. Kakalios, *Phys. Rev. E* **49**, 3610 (1994).
 - [11] K. M. Hill and J. Kakalios, *Phys. Rev. E* **52**, 4393 (1995).
 - [12] K. M. Hill, A. Caprihan, and J. Kakalios, *Phys. Rev. Lett.* **78**, 50 (1997).
 - [13] M. Nakagawa, S. A. Altobelli, A. Caprihan, and E. Fukushima, *Chem. Engineering Science* **52**, in press (1997).
 - [14] K. M. Hill, A. Caprihan, and J. Kakalios, *Axial Segregation of Granular Media Rotated in a Drum Mixer: Pattern Evolution*, preprint, 1997.
 - [15] O. R. Walton and R. L. Braun, in *Proceedings of the joint DOE/NFS workshop on FLOW OF PARTICULATES AND FLUIDS*, edited by M. Roco and S. Plaszynski (Ithaca, New York, 1993).
 - [16] G. H. Ristow, *Europhys. Lett.* **28**, 97 (1994).
 - [17] G. Baumann, I. Janosi, and D. E. Wolf, *Europhys. Lett.* **27**, 203 (1994).

- [18] G. Baumann, I. M. Janosi, and D. E. Wolf, Phys. Rev. E **51**, 1879 (1995).
- [19] V. Buchholtz, T. Pöschel, and H. J. Tillemans, Physica A **216**, 199 (1995).
- [20] G. H. Ristow, Europhys. Lett. **34**, 263 (1996).
- [21] C. M. Dury and G. H. Ristow, J. Phys. I France **7**, 737 (1997).
- [22] G. Metcalfe, T. Shinbrot, J. J. McCarthy, and J. M. Ottino, Nature **374**, 39 (1995).
- [23] M. Nakagawa, S. Altobelli, A. Caprihan, E. Fukushima, and E.-K. Jeong, Experiments in Fluids **16**, 54 (1993).
- [24] O. Zik, D. Levine, S. G. Lipson, S. Shtrikman, and J. Stavans, Phys. Rev. Lett. **73**, 644 (1994).
- [25] J. Schäfer, S. Dippel, and D. E. Wolf, J. Phys. I France **6**, 5 (1996).
- [26] G. H. Ristow, in *Annual Reviews of Computational Physics I*, edited by D. Stauffer (World Scientific, Singapore, 1994), p. 275.
- [27] S. F. Foerster, M. Y. Louge, H. Chang, and K. Allia, Phys. Fluids **6**, 1108 (1994).
- [28] D. V. Khakhar, J. J. McCarthy, T. Shinbrot, and J. M. Ottino, Phys. Fluids **9**, 31 (1997).
- [29] W. Hager, S. Linz, and P. Hänggi, in *Friction, Arching, Contact Dynamics*, edited by D. E. Wolf and P. Grassberger (World Scientific, Singapore, 1997), p. 317.
- [30] C. M. Dury, G. H. Ristow, and M. Nakagawa, in *Powders & Grains 97*, edited by R. P. Behringer and J. T. Jenkins (Balkema, Rotterdam, 1997), p. 499.
- [31] C. Tang and P. Bak, Phys. Rev. Lett. **60**, 2347 (1988).
- [32] F. Cantelaube, Ph.D. thesis, University of Rennes I, Rennes, France, 1995.
- [33] R. Peralta-Fabi, E. Morales, and V. Romero-Rochin, in *Powders & Grains 97*, edited by R. P. Behringer and J. T. Jenkins (Balkema, Rotterdam, 1997), p. 499.

g [m/s ²]	1.62	3.73	9.81	13.6	25.1	274
Θ [°]	48.2	41.4	35.0	33.3	30.2	18.4
ζ/R	0.291	0.274	0.277	0.269	0.283	0.260

TABLE I. Angle of repose, Θ , in the drum middle and dimensionless characteristic length, ζ/R , as function of gravity, g (simulation).

Figure Captions

Figure 1 (a) Flat surface for low rotation speeds, (b) deformed surface for medium rotation speeds with two straight lines added as approximation and (c) fully developed S-shaped surface for higher rotation speeds.

Figure 2 Experimentally measured starting (\circ) and stopping (\star) angle and dynamic angle of repose (\bullet) for mustard seeds.

Figure 3 Dynamic angle of repose for black (\bullet) and yellow (\circ) mustard seeds.

Figure 4 Dynamic angle of repose for small (\bullet) and large (\circ) glass beads.

Figure 5 Comparison of dynamic angle of repose for large mustard seeds taken from MRI (\circ) and non-MRI (\star) measurements.

Figure 6 Comparison of dynamic angle of repose for large mustard seeds taken from MRI (\circ), numerical simulation (\bullet) and the theory of Zik et al. [24] ($—$).

Figure 7 Profile of the dynamic angle of repose along the rotation axis for 2.5 mm spheres: (\bullet) simulation, ($—$) fit.

Figure 8 Dynamic angle of repose as function of sphere diameter for $\Omega = 20$ rpm (simulation); (\star) end cap, (\bullet) drum middle, ($—$) arcus-tangent fit.

Figure 9 Dimensionless range of boundary effect for spheres with different diameter; (\star) $R = 3.5$ cm, (\circ) $R = 7$ cm, (\bullet) $R = 10.5$ cm, dotted line shows value $\zeta = 0.28 R$ for radius-independent regime (simulation).

Figure 10 Range of boundary effect measured in sphere diameters for spheres with different diameter; (\star) $R = 3.5$ cm, (\circ) $R = 7$ cm, (\bullet) $R = 10.5$ cm, ($—$) exponential fit (simulation).

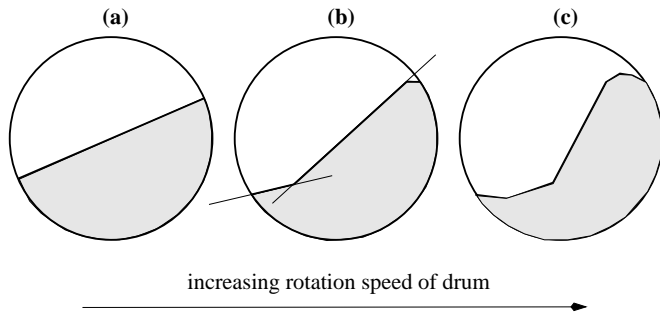


FIG. 1.

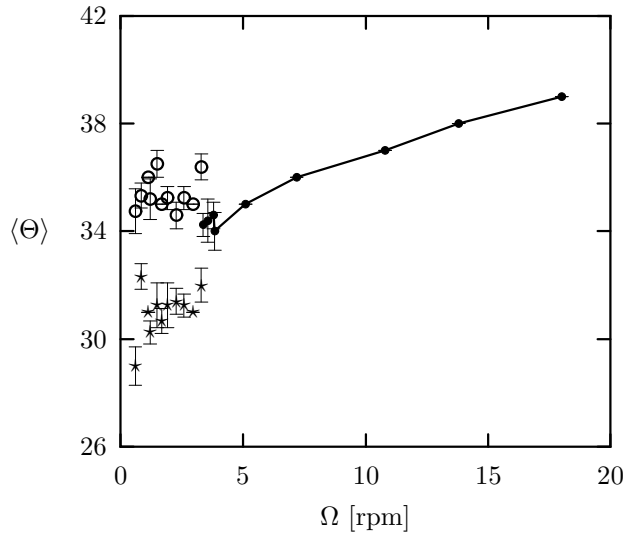


FIG. 2.

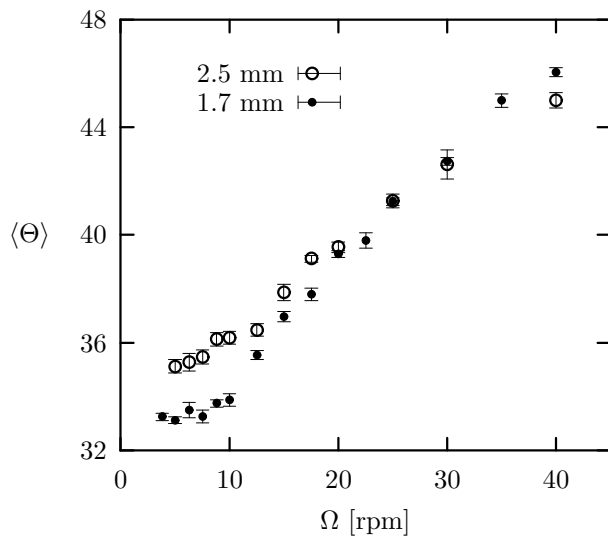


FIG. 3.

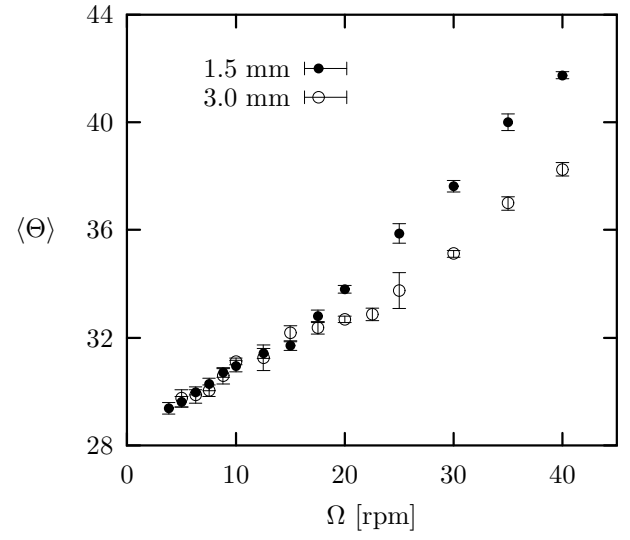


FIG. 4.

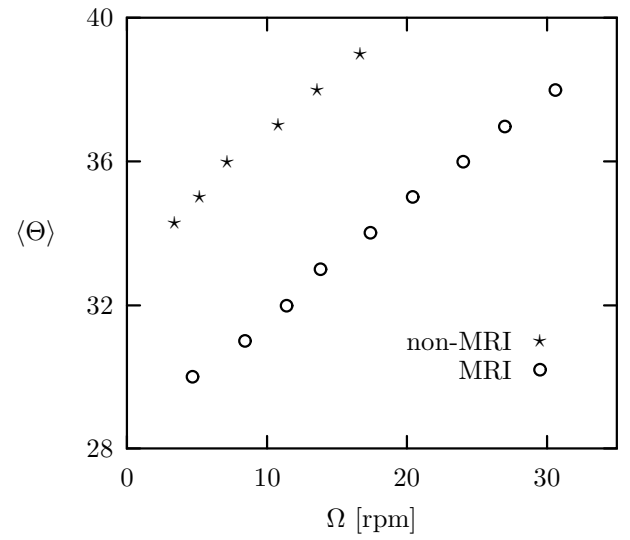


FIG. 5.

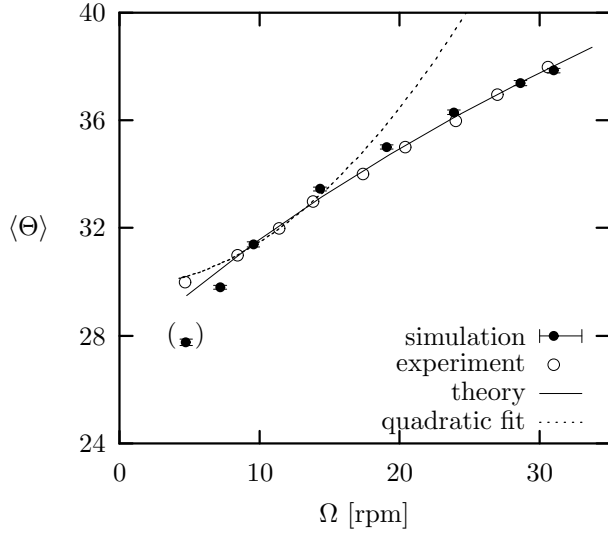


FIG. 6.

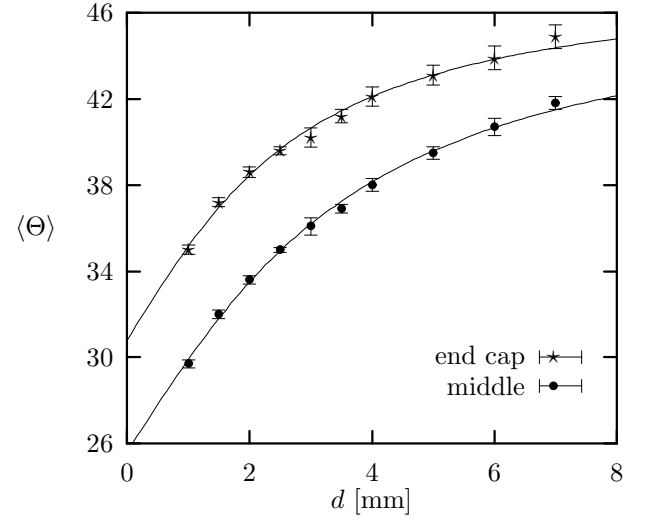


FIG. 8.

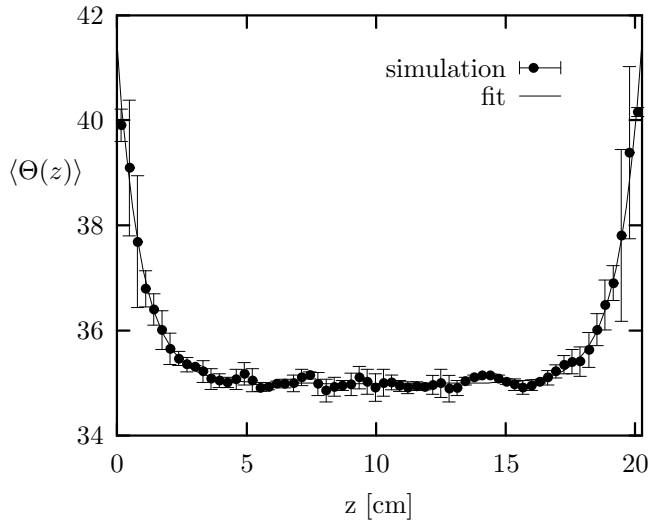


FIG. 7.

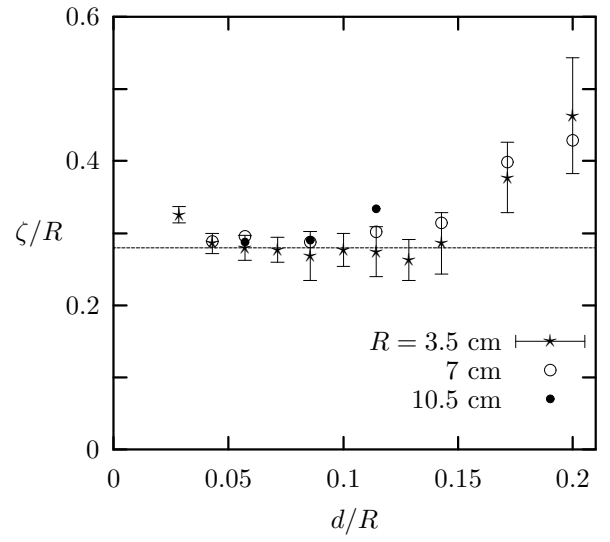


FIG. 9.

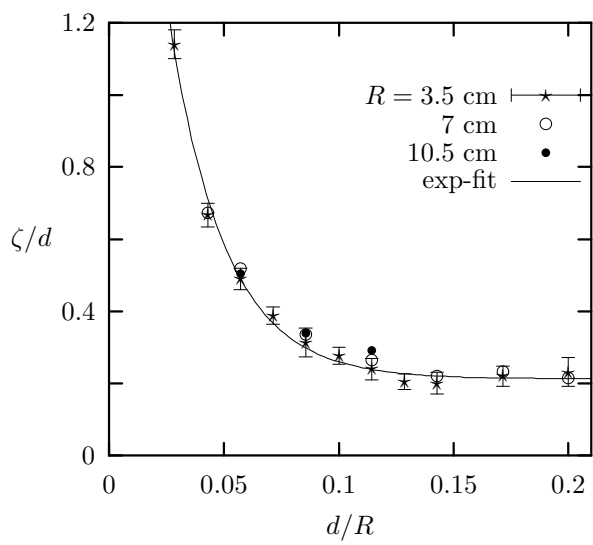


FIG. 10.